



Automatic recognition of SEM microstructure and phases of steel using LBP and random decision forest operator

Subir Gupta^{a,b}, Jit Sarkar^c, M. Kundu^b, N.R. Bandyopadhyay^b, Subhas Ganguly^{d,*}

^a Department of Master of Computer Application, B C Roy Engineering College, Durgapur, West Bengal 713206, India

^b School of Materials Science and Engineering, Indian Institute of Engineering Science and Technology, Shibpur, Howrah, West Bengal 711103, India

^c Boldink Technologies Private Limited, Howrah, West Bengal 711110, India

^d Department of Metallurgical Engineering, National Institute of Technology Raipur, Chhattisgarh 492010, India

ARTICLE INFO

Article history:

Received 6 June 2019

Received in revised form 20 October 2019

Accepted 29 October 2019

Available online 4 November 2019

Keywords:

Automatic recognition of microstructure

SEM microstructure of steel

Local binary pattern

Random decision forest

Feature extraction

Segmentation

ABSTRACT

In this paper, we present a computational model for recognition of steel type i.e., ferrite-pearlite and martensite-austenite grade steel by image processing of scanning electron microscopy (SEM) micrographs followed by phase identification, segmentation and quantification. For this purpose a comprehensive SEM microstructure database were produced through in-house experiments. The diversity in the database in terms of volume fraction, grain refinement and resolution in the microstructure images were achieved through annealing, normalizing and quenching treatments to four different plain carbon steel, containing 0.1, 0.22, 0.35 and 0.48 wt. %C and capturing the images at different magnification (500×, 1000×, 1500×, 2000×, 3000× and 5000×) in SEM under secondary electron (SE) mode. The image processing schedule for this work was developed employing the Gabor filtering, local binary pattern (LBP), random decision forest (RDF) and Otsu thresholding techniques for the purpose of noise reduction, statistical feature extraction, classifier design and segmentation respectively. The prediction accuracy of steel type was found to be significantly high. In case of ferrite-pearlite type steel, the predicted pearlite fractions for the steel containing 0.1, 0.22, 0.35 and 0.48 wt. %C were found to be 0.23 ± 0.02 , 0.3 ± 0.03 , 0.55 ± 0.03 and 0.65 ± 0.03 respectively for the investigated range of magnification (500×–5000×). Similarly, in case of martensite-austenite type steel, the predicted fractions of martensite for the steel containing 0.1, 0.22, 0.35 and 0.48 wt. %C were found to be 0.59 ± 0.02 , 0.52 ± 0.01 , 0.45 ± 0.01 and 0.56 ± 0.02 respectively within the magnification range of 500× to 5000×.

© 2019 Elsevier Ltd. All rights reserved.

1. Introduction

The most challenging part in the advancement of computer aided manufacturing system is to replace the human expertise based skills by means of computer. However, interpretation, and quantitative analysis of micrographs are primarily based on manual observations and skills. This has been intensively used for years in steel microscopic investigation to correlate with the properties of steels aiming to tailor the manufacturing system as per the target requirement. The limitation of human knowledge dependent subjectivity originates the complexity. This is possibly the main bottleneck in advancement and automation of steel processing based manufacturing systems, such as steel casting, rolling, forging, extrusion etc. Thus, the computer assisted quantitative analysis of microstructure in steel emerges as an important area of

research [1–3]. On the other hand, the secondary electron (SE) imaging has been extensively used as a primary technique to investigate the microstructures of steel sample using scanning electron microscopy (SEM). In a SEM, SE image of a suitably etched flat polished surface of steel sample is an area intensity map in the analog domain. Each image pixel displays a corresponding point on the sample. The pixel value is directly proportional to the signal intensity captured by the secondary electron collector at each specific point during scanning [4]. Thus it allows forming the individual phase like ferrite, pearlite, martensite, bainite etc. with differentiated grayscale contrast region in the microstructure image. The manual quantitative metallography, especially for steel SEM microstructure, is still complicated, difficult, tedious and time-consuming task. Number of commercial image analyzer software exists and are used to determine the grain size, phase fraction and phase segmentation of metallographic images. The task like phase identification, grain boundary detection etc. specifically to steel microstructure image still remain human skill dependent.

* Corresponding author.

E-mail address: sganguly.met@nitrr.ac.in (S. Ganguly).

This is because of the possibility of presence of many different phases with close similarity in contrast and morphology in the steel micrograph which is difficult to discriminate.

Therefore, the research in quantitative metallography of steel is a pragmatic need. The subject has attracted the attention of researcher for developing the application of computer based smart system that can accomplish the problem for automatic identification and quantification of phases present in a metallographic image, determination and analysis of grain boundaries along with the conventional quantitative metallographic information [3,5]. In this context, good amount of research is in progress with focus on prediction of phase fractions, phase orientation, phase morphology, inclusions and identifying precipitate etc. in steel as well other metallic materials in general [6–10].

Many works have been reported related to SEM microstructure image processing using different computational techniques. In this regards, it is worth to mention that DeCost et al. [11] have used 'bag of visual features' based methods applied to wide range of microstructural images for automatic recognition and classification of microstructure. In this work, application of the support vector machine (SVM) has been found to be an efficient technique for microstructure classification task. On the other hand, Hecht et al. [12] studied the carbide network in steel using image processing techniques. Nevertheless, these research calls for further development of more efficient and effective computer-assisted algorithms and systems for smart analysis of microstructural images. A plausible image processing technique is therefore needed for effective analysis and interpretation of steel microstructures. Different techniques have already been proposed to acquire and enhance images of steel microstructure for industrial importance. It has been established that the statistical tools are very effective in noise reduction along with pattern recognition, feature extraction and segmentation [13], while maintaining a satisfactory level of accuracy in image analysis. Recent fast development of computer techniques improve image processing remarkably and provide the further opportunity to improvise the SEM microstructure image processing algorithms [2,14–16].

This paper proposed a comprehensive image processing procedure applicable for steel microstructure image. The effort has been made for automatic detection of steel type, i.e., ferrite-pearlite/martensite-austenite and followed by the identification and quantification of the phases present. For this purpose local binary pattern, random forest and Otsu operators are used in order to extract features, classification model and segmentation of microstructure images [17–19]. The procedure has been aimed to address for four different steels and a wide range of magnification from 500× to 5000×. The proposed procedure for automatic detection and quantification of microstructures will contribute to the development of computerized system capable of replacing the human-skill based task and promoting the development of framework for Industry 4.0 in steel processing industries.

2. The microstructure data and image processing model

2.1. SEM image data set

To propose the algorithm for processing and analyzing of different SEM images, it requires large dataset comprising of ferrite-pearlite and martensite-austenite microstructures having different volume fractions and at different magnifications. To obtain such dataset, plain carbon steel containing 0.1, 0.22, 0.35 and 0.48 wt. %C have been subjected to annealing, normalizing and quenching treatment followed by etching with 2% nital solution to obtain different volume fractions of ferrite-pearlite and martensite-austenite microstructures and the SEM images in SE mode have been captured at 500×, 1000×, 1500×, 2000×, 3000× and 5000× magnification for further processing. The ferrite and pearlite regions and the austenite and martensite regions in the micrographs appears to be white and dark respectively.

2.2. Noise reduction and contrast enhancement

The original SEM images of the two different grades of steel have been subjected to noise reduction using Gabor filtering before

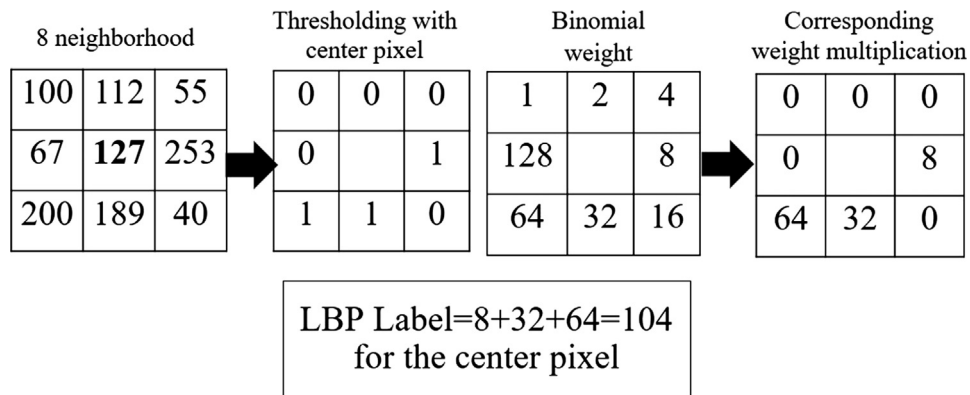
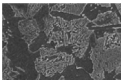
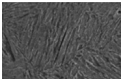


Fig. 1. The step by step computation of 8 neighborhood LBP label.

Table 1
Statistical feature value obtained from the training set of microstructures for both steels.

Microstructure	Mean	SD	Kurtosis	Skewness	Entropy	Class of Microstructure
	6.960134	0.61443	3.572716	0.074484	4.065534	Ferrite-Pearlite
	6.14776	0.950834	2.619272	0.058051	2.804971	Martensite-Austenite

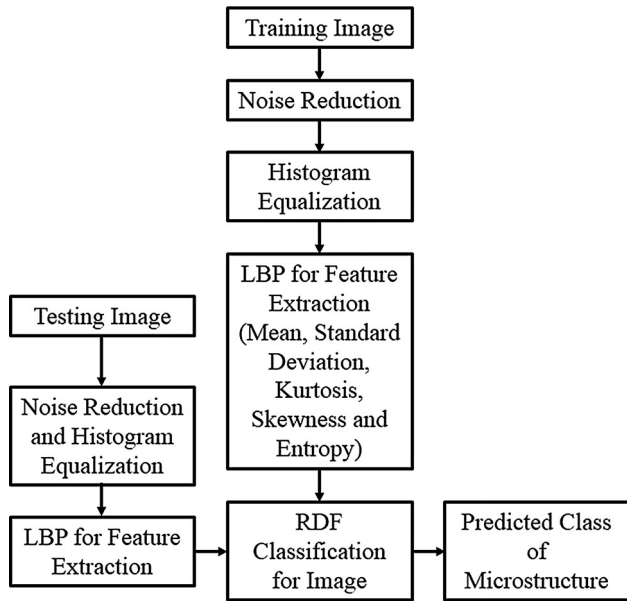


Fig. 2. The schematic flow diagram of the overall microstructure image analysis procedure proposed in this work for the prediction of steel microstructure class.

any further image processing stages. Gabor filtering uses a linear filter for texture analysis in a localized region around a point or region of interest. It analyzes for the presence of any specific frequency content in images along specific direction. For extracting significant features from images, a set of Gabor filters with

different frequencies and orientations may prove to be very useful. On the other hand, in microstructure images the improper sample preparation and differential chemical etching causes contrast sensitive noises in SEM micrographs. Therefore, the Gabor tool is found to be an efficient technique for noise reduction in context of the present application. Two-dimensional Gabor filters in the discrete domain are represented by the following equations [20]:

$$G_C[i, j] = B e^{-\frac{(i^2 + j^2)}{2\sigma^2}} \cos(2\pi f(\text{icos}\theta + \text{jsin}\theta)) \quad (1)$$

$$G_S[i, j] = C e^{-\frac{(i^2 + j^2)}{2\sigma^2}} \sin(2\pi f(\text{icos}\theta + \text{jsin}\theta)) \quad (2)$$

where, B and C are the normalizing factors which are need to determined, f is the frequency in the texture to be searched, θ is the texture oriented in a particular direction, σ is the basis support or the size of the image region being analyzed.

The noise reduction of the original SEM images have been followed by their histogram equalization, an image processing technique for contrast enhancement of the images using the histogram of the noise-reduced images. It increases the global contrast of images whose usable data are represented by close contrast values. Let us consider a discrete grayscale image $\{x\}$ and let n_i represent the number of occurrences of gray level i . Then the probability of an occurrence of a pixel of level i in the image is defined by the following equation [21]:

$$p_x(i) = p(x = i) = \frac{n_i}{n}, \quad 0 \leq i < L \quad (3)$$

where, L represent the total number of gray levels in the image, n is the total number of pixels in the image, and $p_x(i)$ is the image's

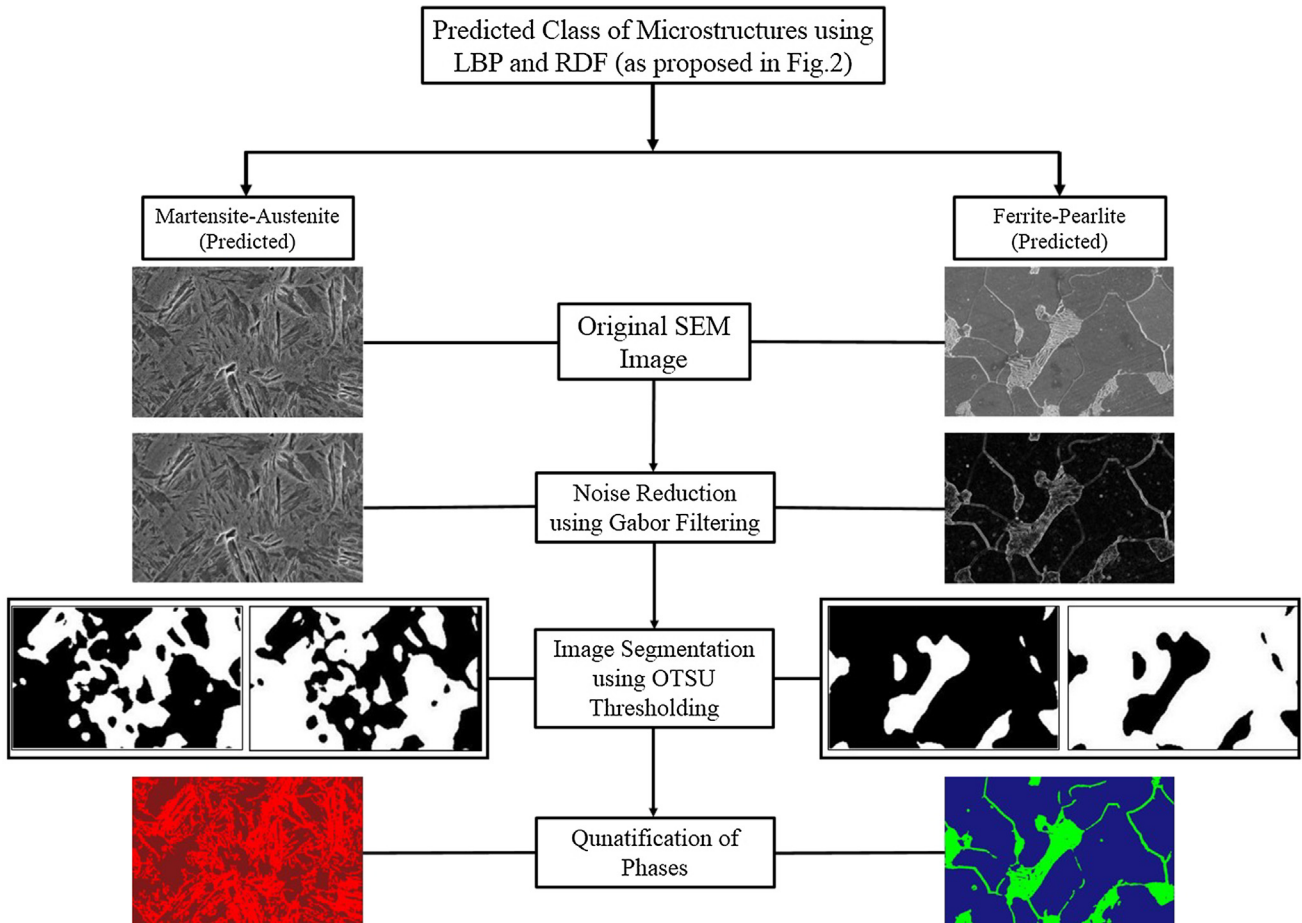


Fig. 3. Phase segmentation and quantification after the class has been predicted by the proposed LBP and RDF based model for steel microstructure class identification.

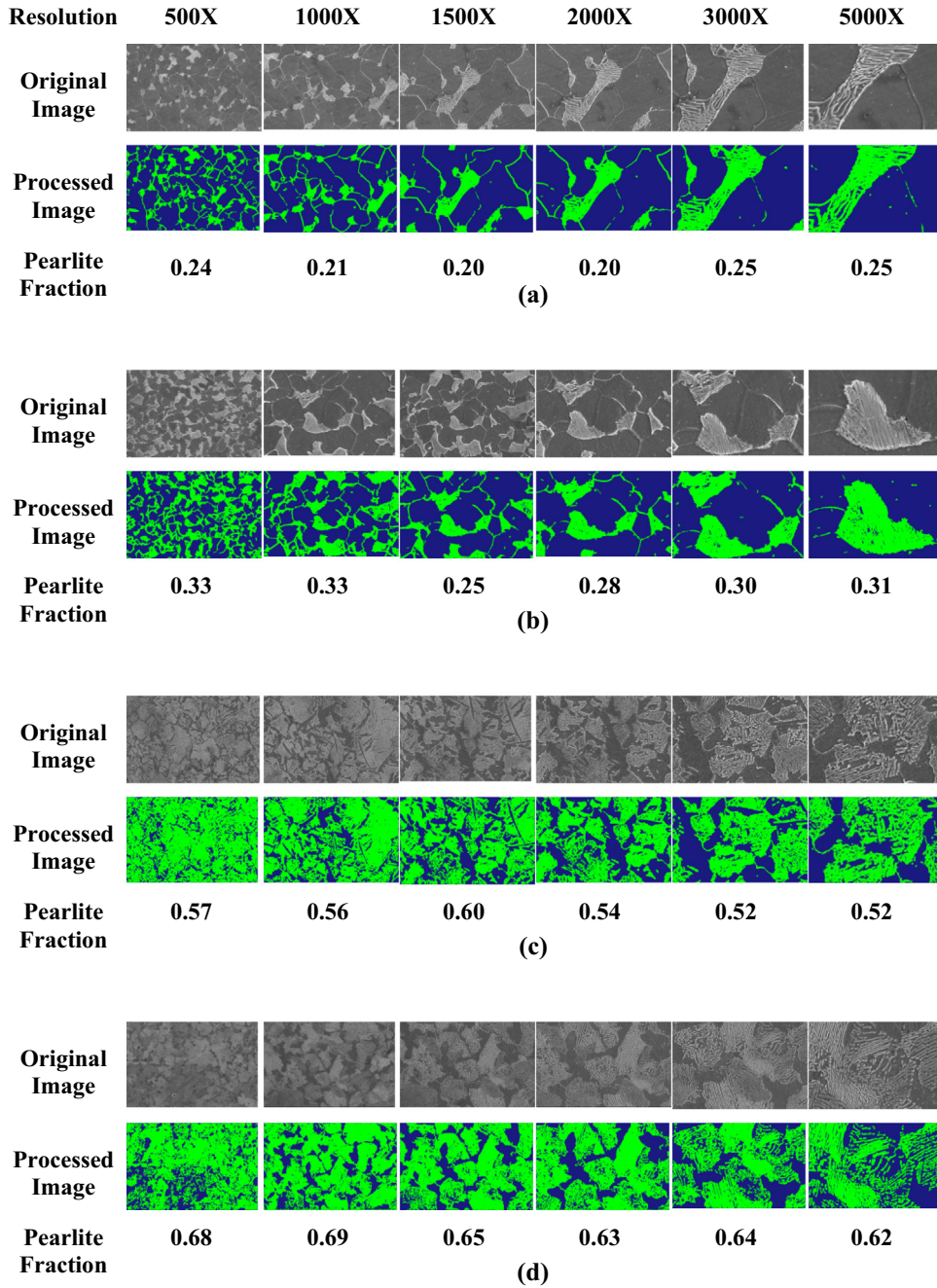


Fig. 4. The prediction of steel class, segmentation and quantification results with the variation of magnification (500–5000×) of SEM microstructures of ferrite-pearlite type steel samples containing (a) 0.1 wt. %C, (b) 0.22 wt. %C, (c) 0.35 wt. %C and (d) 0.48 wt. %C.

histogram for pixel value i , normalized to $\{0,1\}$. The cumulative distribution function corresponding to p_x which represent the image's accumulated normalized histogram and is defined by the following equation:

$$cdf_x(i) = \sum_{j=0}^i p_x(j) \quad (4)$$

2.3. LBP feature extraction

The Local Binary Pattern is an image operator based on local pixel information and complementary to the contrast information [18]. The LBP operator represents the image as an array or image of integer levels allowing a reduced scale representation of the image.

These integer labels or their statistics are significantly used in respect of analysis of the image. This characteristics allows to consider the tool for feature extraction in the present application of image processing procedure in microstructure image analysis. The original LBP operator functions on a 3×3 pixel block i.e., 8 neighborhood pixels, for an image. A label for the center pixel is obtained by the approach described in Fig. 1. The neighborhood pixels in the block are first thresholded with its center pixel value, followed by multiplication with the corresponding binomial weights. Eventually, it computes the LBP label for center pixel by summing up the values of the resulted matrix. The computation of LBP level can be summarized mathematically as:

$$LBP_{p,r}(N_c) = \sum_{p=0}^{P-1} g(N_p - N_c) 2^p \quad (5)$$

where, neighborhood pixels (N_p) in each block is thresholded by its center pixel value (N_c), p denotes sampling points and r is the radius. The binary threshold function $g(x)$ is defined as:

$$g(x) = \begin{cases} 0, & x < 0 \\ 1, & x \geq 0 \end{cases} \quad (6)$$

The LBP is used in the present work in context of extraction of characteristics features of digitized SEM microstructure. For this purpose, first the LBP labels for each of the pixel have been computed for an image. Then the five statistical attributes such as mean, standard deviation, kurtosis, skewness and entropy of the LBP levels of the image have been extracted for numerical representation of each microstructure image. The detail description of these statistical attributes are available in reference [22]. Such numerical representation of two sample microstructures are shown in Table 1. This five vector numerical representation of total of 72 SEM microstructures have been computed and then used to develop the classifier by random forest technique and subsequent analysis of microstructure. The detail description of the methods are presented in the following subsections.

2.4. Random forest classifier

Random forest is an ensemble classifier, originally proposed for solving classification problems, comprising of number of decision trees. Each of the decision tree participate to yield a separate classification result and accordingly vote for a particular class. The most popular class is then declared as the winner of the game. The method involves a two stage process namely, training and classification. During any training stage the set of decision trees are generated from the number of training images data. Further details about the method is available in reference [18]. The advantage of random forest phase classification method is that the correction for overfitting during training is inherent in the process of training [23]. Especially for this characteristics, it has been used for classification of the present microstructure class.

In the present work, the training set of 72 image data generated by the LBP operator are used to generate the decision trees. The leaf nodes are the steel class i.e. ferrite-pearlite and martensite-austenite type of steel, whereas the root leaf and the branches are the randomly selected subset from the computed five-fold statistical features as stated in the previous section. Each node other than the leaf node is a trial from the selected subset attribute i.e., a statistical feature out of the five in the present application. Thus the classification of the steel class ends at the leaf class and the same trial has been performed for all the decision trees. Eventually, based on the highest voting performance the steel class of an image has been attempted to predict from its LBP features. Once the training has successfully developed the trained set of decision trees, then the test microstructure image data have been subjected to prediction of the steel image class. After this prediction of the steel class, the microstructure images have been processed for binarization using the Otsu segmentation [24]. The details of the segmentation procedure is presented in subsequent section.

2.5. Segmentation and phase quantification

After the successful prediction of the steel class of the images, the presence of combination of two phases in the microstructures are known. In this stage, binarization of the microstructure images have been performed applying the Otsu thresholding operator. The approach adopts clustering-based image thresholding i.e., the grayscale images are reduced to respective binary images. In spite of many segmentation tool Otsu is one of the important and widely used region based segmentation method and it has been preferred for present application of segmentation of microstructure images.

For phase quantification, the input images have been classified as background and object i.e., pearlite or martensite and the volume fraction of the respective phases have been calculated from the final images containing the combination of the separated background and object.

A MATLAB routine has been developed to implement the proposed image processing procedures using the aforesaid tools and the process-flow as described in Fig. 2. The MATLAB routine has been executed in an ordinary desktop computer with configuration of i5 (3rd generation) processor and 4 GB ram in MATLAB 9.0 (R2016a) platform. The average computation time for processing of each microstructure image is 60–90 s.

3. Results and discussions

To demonstrate the effectiveness of the proposed approach, the model has been studied under the test microstructure image dataset. Fig. 3 shows the results in different stages of processing of the SEM images, when applied upon two microstructures of predominantly ferrite-pearlite and martensite-austenite type of steel, determined by the proposed LBP and RDF based model stated above (see Fig. 2). The original microstructures have been processed for identification of steel type i.e., ferrite-pearlite or martensite-austenite type of steel by the RDF classifier based on the five statistical features such as mean, standard deviation, kurtosis, skewness and entropy. The close search-match of the test microstructures predict the steel type of the unknown microstructures. In the later stage, when the steel types have been identified, the microstructures have been processed and analyzed subsequently for phase identification and quantification. The effectiveness and efficiency of identification of steel types along with the recognition of the phase constituents and their quantification for the variation of phase fractions and magnifications are significantly consistent.

Fig. 4 shows the classification and segmentation results of ferrite-pearlite type steel microstructures against the variations of carbon content and the resolution of the images. The corresponding quantification of pearlite phase fractions as against the magnification, for steels containing different carbon content, are summarized in Fig. 5. When the phase fractions have been computed against different magnifications, it has been observed that the predicted pearlite fractions for the steels under investigation are found to be quite consistent against magnification. The pre-

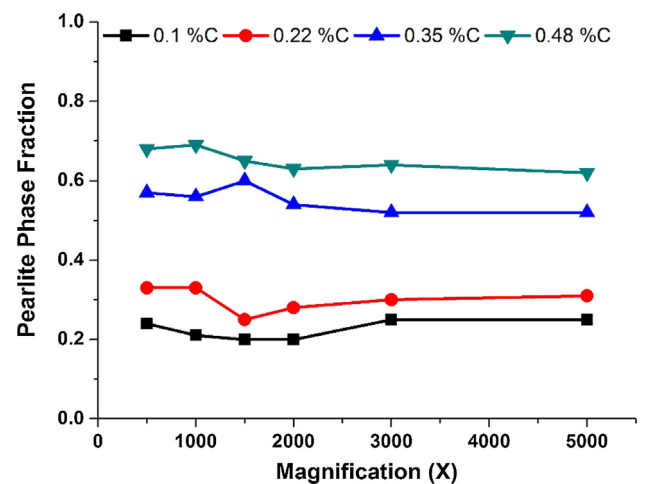


Fig. 5. The variation of the predicted pearlite phase fraction as against the magnification and different carbon content (0.1–0.48 wt. %C) of ferrite-pearlite type steel.

dicted pearlite fractions for the steel containing 0.1, 0.22, 0.35 and 0.48 wt. %C are 0.23 ± 0.02 , 0.3 ± 0.03 , 0.55 ± 0.03 and 0.65 ± 0.03 respectively for the investigated range of magnification ($500\times$ – $5000\times$). Therefore, it indicates that the proposed image analysis approach can achieve the significant level of accuracy for phase quantification of ferrite-pearlite microstructures, independence of wide range of magnification ($500\times$ – $5000\times$). As the fraction ferrite and pearlite are complementary to each other, no separate analysis of ferrite fractions are presented.

As it can be seen from Fig. 5, the variation of pearlite phase fractions in the lower magnifications are relatively higher for all the steels except the steel with 0.1 wt. %C. However, the variation of phase fractions are insignificant for the microstructures at higher resolutions ($>3000\times$). This can be attributed to the difficulty in resolving the pearlite phase at lower magnification which could

not be accurately segmented by the present analysis method. However, in case of low carbon steel, as the pearlite fractions are small, the scope for prediction errors are less which lead to the relatively less chance of variations in the pearlite phase fractions. It is noteworthy that the proposed segmentation qualifies the quantification of pearlite in ferrite-pearlite steel in terms of the variation in carbon composition in steel as well as the wide range of magnifications of the SEM images. Also, the prediction satisfies the physical metallurgical principle of increase in pearlite phase fractions with the increase in carbon content in ferrite-pearlite steel.

The classification and segmentation results of martensite-austenite type steel microstructures as against the variations of carbon content and the resolution of the images are presented in Fig. 6, while the quantification of martensite phase fractions as against the magnification, for steels containing different carbon

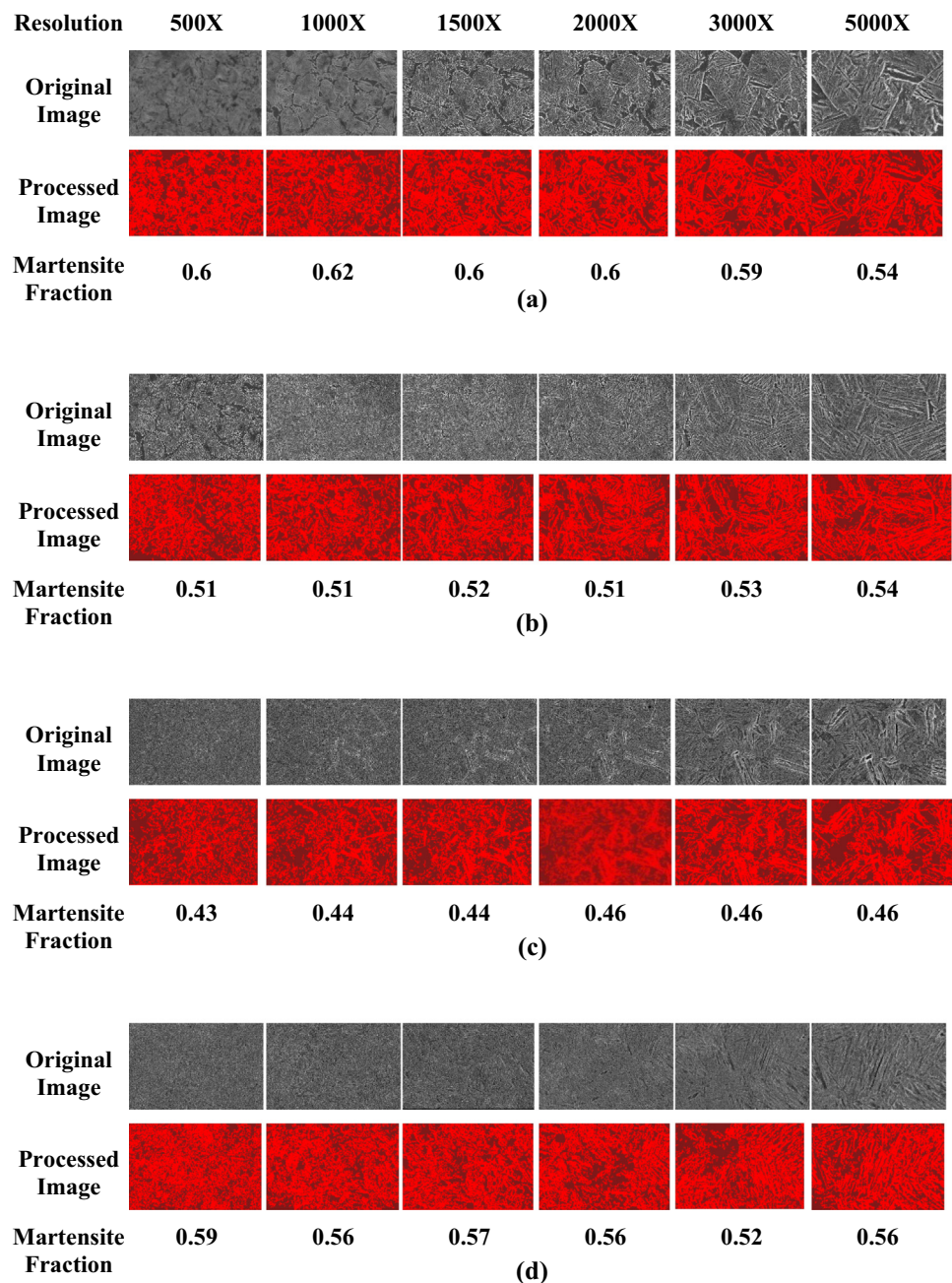


Fig. 6. The prediction of steel class, segmentation and quantification results with the variation of magnification (500 – $5000\times$) of SEM microstructures of martensite-austenite type steel samples containing (a) 0.1 wt. %C, (b) 0.22 wt. %C, (c) 0.35 wt. %C and (d) 0.48 wt. %C.

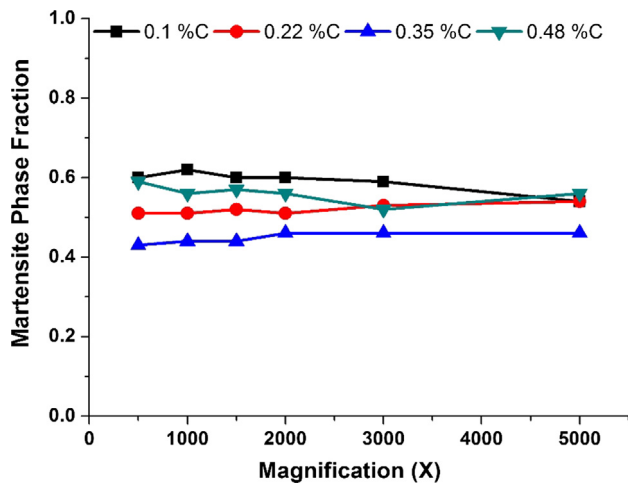


Fig. 7. The variation of the predicted martensite phase fraction as against the magnification and different carbon content (0.1–0.48 wt. %C) of martensite-austenite type steel.

content, are summarized in Fig. 7. In case of martensite-austenite type steel the fractions of martensite for the steel containing 0.1, 0.22, 0.35 and 0.48 wt. %C are predicted with an accuracy of 0.59 ± 0.02 , 0.52 ± 0.01 , 0.45 ± 0.01 and 0.56 ± 0.02 respectively within the magnification range of $500\times$ to $5000\times$.

In case of martensite-austenite type steel, the variations of martensite phase fractions in the steels under consideration are convincingly consistent in general as depicted in Fig. 7. Though in the case of 0.48 wt. %C steel the variation is relatively more as compare to the rest of the cases, particularly in the low magnification regions ($500\times$ to $3000\times$). This may be due to the fact that the martensite structure formation merely depends on the condition of the prior-austenite structure where higher carbon concentration promotes the possibility of the presence of carbides along with the transformed martensite phase due to incomplete dissolution of the carbides during austenitization [25–27]. These undissolved carbides retained along with the martensite phase may be failed to differentiate by the proposed image analysis approach.

4. Conclusions

An image processing framework based on LBP histogram and random decision forest tree has been proposed for effective and efficient classification and segmentation of SEM steel microstructures. The result of conducted analysis is plausibly effective for automatic recognition and quantification of phases in ferrite-pearlite and martensite-austenite type steel microstructures, unlike the available commercial image analyzers. The prediction accuracy of quantification of the martensite and pearlite phase fractions are significantly high and independent of carbon concentration of steel samples and resolution of the SEM microstructures. In case of ferrite-pearlite type steel, the predicted pearlite fractions for the steel containing 0.1, 0.22, 0.35 and 0.48 wt. %C are found to be 0.23 ± 0.02 , 0.3 ± 0.03 , 0.55 ± 0.03 and 0.65 ± 0.03 respectively for the investigated range of magnification ($500\times$ – $5000\times$). Similarly, in case of martensite-austenite type steel, the predicted fractions of martensite for the steel containing 0.1, 0.22, 0.35 and 0.48 wt. %C are found to be 0.59 ± 0.02 , 0.52 ± 0.01 , 0.45 ± 0.01 and 0.56 ± 0.02 respectively within the magnification range of $500\times$ to $5000\times$. It was found that the segmentation process works effectively and efficiently for both ferrite-pearlite and martensite-austenite type steels with varying carbon content from 0.1 to 0.48 wt. %C and over a wide range of magnification of $500\times$

to $5000\times$ and thus can be useful in prediction of the pearlite and martensite phase fractions in the mentioned steel types. The efficiency of the segmentation procedure allows to achieve the proper prediction of the variation of phase fractions within the standard deviation from 0.01 to 0.03 over the magnification range of $500\times$ to $5000\times$ indicating a high level of accuracy. The proposed image analysis procedure proven to be effective for use in a plausible range of steel compositions and magnifications. Nevertheless, incorporation of more categories of steel microstructures remain beyond the scope of the present work due to limitations of complexity in the basic approach and the non-availability of microstructure data. Scope exist for further extension of the present work to address the problem of incorporation of more complex steel microstructures.

5. Data availability

The raw/processed data required to reproduce these findings cannot be shared at this time as the data also forms part of an ongoing study.

Conflict of interest

The authors declare that there is no conflict of interest in the present work.

References

- [1] T. Wejrzanowski, W. Spychalski, K. Różniatowski, K. Kurzydłowski, Image Based Analysis of Complex Microstructures of Engineering Materials, *Int. J. Appl. Math. Comput. Sci.* 18 (2008) 33–39, <https://doi.org/10.2478/v10006-008-0003-1>.
- [2] C. Liu, B. Shi, J. Zhou, C. Tang, Quantification and characterization of microporosity by image processing, geometric measurement and statistical methods: Application on SEM images of clay materials, *Appl. Clay Sci.* 54 (2011) 97–106, <https://doi.org/10.1016/j.clay.2011.07.022>.
- [3] B.L. DeCost, B. Lei, T. Francis, E.A. Holm, High Throughput Quantitative Metallography for Complex Microstructures Using Deep Learning: A Case Study in Ultrahigh Carbon Steel, *Microsc. Microanal.* 25 (2019) 21–29, <https://doi.org/10.1017/S1431927618015635>.
- [4] H.S. Wong, M.K. Head, N.R. Buenfeld, Pore segmentation of cement-based materials from backscattered electron images, *Cem. Concr. Res.* 36 (2006) 1083–1090, <https://doi.org/10.1016/j.cemconres.2005.10.006>.
- [5] B.L. DeCost, T. Francis, E.A. Holm, Exploring the microstructure manifold: Image texture representations applied to ultrahigh carbon steel microstructures, *Acta Mater.* 133 (2017) 30–40, <https://doi.org/10.1016/j.actamat.2017.05.014>.
- [6] Phase Determination in Low Carbon Steel Metallographic Image Using Wavelet Transform, *Image (Rochester, N.Y.)*, 21 (2009) 125–129.
- [7] J. Adamczyk, A. Grajcar, Heat treatment and mechanical properties of low-carbon steel with dual-phase microstructure, *J. Achiev. Mater.* 22 (2007) 13–20, http://www.journalamme.org/papers_vol22_1/1010.pdf.
- [8] S. Banerjee, S.K. Ghosh, S. Datta, S.K. Saha, Segmentation of dual phase steel micrograph: An automated approach, *Meas. J. Int. Meas. Confed.* 46 (2013) 2435–2440, <https://doi.org/10.1016/j.measurement.2013.04.057>.
- [9] S.G. Lee, Y. Mao, A.M. Gokhale, J. Harris, M.F. Horstemeyer, Application of digital image processing for automatic detection and characterization of cracked constituent particles/inclusions in wrought aluminum alloys, *Mater. Charact.* 60 (2009) 964–970, <https://doi.org/10.1016/j.matchar.2009.03.014>.
- [10] W.B. Liewers, A.K. Pilkey, An evaluation of global thresholding techniques for the automatic image segmentation of automotive aluminum sheet alloys, *Mater. Sci. Eng. A* 381 (2004) 134–142, <https://doi.org/10.1016/j.msea.2004.04.002>.
- [11] B.L. Decost, E.A. Holm, A computer vision approach for automated analysis and classification of microstructural image data, *Comput. Mater. Sci.* 110 (2015) 126–133, <https://doi.org/10.1016/j.commatsci.2015.08.011>.
- [12] M.D. Hecht, B.A. Webler, Y.N. Picard, Digital image analysis to quantify carbide networks in ultrahigh carbon steels, *Mater. Charact.* 117 (2016) 134–143, <https://doi.org/10.1016/j.matchar.2016.04.012>.
- [13] W. Li, Z. Zhu, F. Jiang, G. Zhou, G. Chen, Fault diagnosis of rotating machinery with a novel statistical feature extraction and evaluation method, *Mech. Syst. Signal Process.* 50–51 (2015) 414–426, <https://doi.org/10.1016/j.ymssp.2014.05.034>.
- [14] A. Campbell, P. Murray, E. Yakushina, S. Marshall, W. Ion, New methods for automatic quantification of microstructural features using digital image processing, *Mater. Des.* 141 (2018) 395–406, <https://doi.org/10.1016/j.matdes.2017.12.049>.

- [15] E.G. Ioanid, A. Ioanid, B.T. Goras, L. Goras, Assessment of the cleaning effect of HF cold plasma by statistical processing of photographic image, *Meas. J. Int. Meas. Confed.* 46 (2013) 2569–2576, <https://doi.org/10.1016/j.measurement.2013.03.020>.
- [16] F. Abed, Microstructural Analysis of Failure in Building Materials, *Int. J. Eng. Technol.* 2 (2012) 1027–1031.
- [17] B. Yang, S. Chen, A comparative study on local binary pattern (LBP) based face recognition: LBP histogram versus LBP image, *Neurocomputing* 120 (2013) 365–379, <https://doi.org/10.1016/j.neucom.2012.10.032>.
- [18] L. Breiman, Random Forests, *Mach. Learn.* 45 (2001) 5–32, <https://doi.org/10.1023/A:1010933404324>.
- [19] P.S. Liao, T.S. Chen, P.C. Chung, A fast algorithm for multilevel thresholding, *J. Inf. Sci. Eng.* 17 (2001) 713–727.
- [20] S.L. Liu, Z.D. Niu, G. Sun, Z.P. Chen, Gabor filter-based edge detection: A note, *Optik (Stuttg.)* 125 (2014) 4120–4123, <https://doi.org/10.1016/j.ijleo.2014.01.102>.
- [21] R. Hummel, Image enhancement by histogram transformation, *Comput. Graph. Image Process.* 6 (2008) 184–195, [https://doi.org/10.1016/s0146-664x\(77\)80011-7](https://doi.org/10.1016/s0146-664x(77)80011-7).
- [22] X. Qing, Y. Jie, D. Siyi, Texture segmentation using LBP embedded region competition, *Electron. Lett. Comput. Vis.* 5 (2005) 41–47, <http://elcvia.cvc.uab.es/article/download/83/65>.
- [23] V.Y. Kulkarni, P.K. Sinha, Effective Learning and Classification using Random Forest Algorithm, *Int. J. Eng. Innov. Technol.* 3 (2014) 267–273.
- [24] T. Dutta, D. Das, S. Banerjee, S.K. Saha, S. Datta, An automated morphological classification of ferrite-martensite dual-phase microstructures, *Meas. J. Int. Meas. Confed.* 137 (2019) 595–603, <https://doi.org/10.1016/j.measurement.2018.12.106>.
- [25] S.M.C. van Bohemen, J. Sietsma, Martensite formation in partially and fully austenitic plain carbon steels, *Metall. Mater. Trans. A Phys. Metall. Mater. Sci.* 40 (2009) 1059–1068, <https://doi.org/10.1007/s11661-009-9796-2>.
- [26] S.M.C. van Bohemen, J. Sietsma, Kinetics of martensite formation in plain carbon steels: critical assessment of possible influence of austenite grain boundaries and autocatalysis, *Mater. Sci. Technol.* 30 (2014) 1024–1033, <https://doi.org/10.1179/1743284714y.00000000532>.
- [27] C. Celada-Casero, J. Sietsma, M.J. Santofimia, The role of the austenite grain size in the martensitic transformation in low carbon steels, *Mater. Des.* 167 (2019), <https://doi.org/10.1016/j.matdes.2019.107625> 107625.